Draft version February 25, 2022
Typeset using LaTeX **modern** style in AASTeX62

arXiv:1808.04294v1 [astro-ph.HE] 13 Aug 2018

NICER Discovers mHz Oscillations in the "Clocked" Burster GS 1826-238

T. E. Strohmayer,[1] K. C. Gendreau,[2] D. Altamirano,[3] Z. Arzoumanian,[2] P. M. Bult,[4] D. Chakrabarty,[5] J. Chenevez,[6] S. Guillot,[7,8] T. Guver,[9,10] J. Homan,[11,12] G. K. Jaisawal,[6] L. Keek,[13] S. Mahmoodifar,[1] J. M. Miller,[14] and F. Ozel[15]

[1] *Astrophysics Science Division and Joint Space-Science Institute, NASA's Goddard Space Flight Center, Greenbelt, MD 20771, USA*

[2] *X-ray Astrophysics Laboratory, Astrophysics Science Division, NASA's Goddard Space Flight Center, Greenbelt, MD 20771, USA*

[3] *Physics & Astronomy, University of Southampton, Southampton, Hampshire SO17 1BJ, UK*

[4] *Astrophysics Science Division, NASA's Goddard Space Flight Center, Greenbelt, MD 20771, USA*

[5] *MIT Kavli Institute for Astrophysics and Space Research, Massachusetts Institute of Technology, Cambridge, MA 02139, USA*

[6] *National Space Institute, Technical University of Denmark, Elektrovej 327-328, DK-2800, Lyngby, Denmark*

[7] *CNRS, IRAP, 9 avenue du Colonel Roche, BP 44346, F-31028 Toulouse Cedex 4, France*

[8] *Université de Toulouse, CNES, UPS-OMP, F-31028 Toulouse, France*

[9] *Istanbul University, Faculty of Science, Department of Astronomy and Space Sciences, Beyazıt, 34119, Istanbul, Turkey*

[10] *Istanbul University Observatory Research and Application Center, Beyazıt, 34119 Istanbul, Turkey*

[11] *Eureka Scientific, Inc., 2452 Delmer Street, Oakland, CA 94602, USA*

[12] *SRON, Netherlands Institute for Space Research, Sorbonnelaan 2, 3584 CA Utrecht, The Netherlands*

[13] *Department of Astronomy, University of Maryland College Park, MD 20742, USA*

[14] *Department of Astronomy, University of Michigan, 1085 South University Ave, Ann Arbor, MI 48109-1107, USA*

[15] *Astronomy Department, University of Arizona, 933 N. Cherry Ave., Tucson, AZ 85721, USA*

ABSTRACT

We report the discovery with the *Neutron Star Interior Composition Explorer* (*NICER*) of mHz X-ray brightness oscillations from the "clocked burster" GS 1826−238. *NICER* observed the source in the periods 2017 June 20 - 29, July 11 - 13, and September 9 - 15, for a total useful exposure of 34 ks. Two consecutive dwells obtained on 2017 September 9 revealed highly significant oscillations at a frequency of 8 mHz. The fractional, sinusoidal modulation amplitude increases from 0.7% at 1 keV to $\approx$ 2% at 6 keV. Similar oscillations were also detected at lower significance in three additional dwells. The oscillation frequency and amplitude are consistent with those of mHz QPOs reported in other accreting neutron star systems. A thermonuclear X-ray burst was also observed on 2017 June 22. The burst properties and X-ray colors are both consistent with GS 1826 being in a soft spectral state during these observations, findings that are confirmed by ongoing monitoring with *MAXI* and *SWIFT*-BAT. Assuming that the mHz oscillations are associated with black body emission from the neutron star surface, modeling of the phase-resolved

spectra shows that the oscillation is consistent with being produced by modulation of the temperature component of this emission. In this interpretation, the black body normalization, proportional to the emitting surface area, is consistent with being constant through the oscillation cycle. We place the observations in the context of the current theory of marginally stable burning and briefly discuss the potential for constraining neutron star properties using mHz oscillations.

Keywords: stars: neutron — stars: oscillations — stars: rotation — X-rays: binaries — X-rays: individual (GS 1826−238) — methods: data analysis

1. INTRODUCTION

Neutron stars in accreting X-ray binaries are known to exhibit phenomena associated with unstable nuclear burning on their surfaces. At present we know of 111 such systems[1] (Galloway & Keek 2017). These objects produce hydrogen and helium-powered thermonuclear X-ray flashes, also known as Type I X-ray bursts (Strohmayer & Bildsten 2006), as well as the longer and rarer "superbursts," likely powered by carbon burning (Strohmayer & Brown 2002; Cumming & Bildsten 2001). A much smaller number of objects, five at present count, have shown low-frequency ($\approx 7-10$ mHz) oscillations very likely associated with the transition from stable to unstable burning, known as marginally stable nuclear burning (Heger et al. 2007b; Galloway & Keek 2017).

Revnivtsev et al. (2001) reported the first detections of mHz quasiperiodic oscillations (QPOs) in three accreting neutron star systems, 4U 1608−52, 4U 1636−536, and Aql X-1. They argued that the mHz oscillations were very likely associated with the neutron star surface and not the accretion flow. They also showed that they only occur within a narrow range of X-ray luminosity. Since then, mHz oscillations have also been reported from 4U 1323−619 (Strohmayer & Altamirano 2012), and the 11 Hz pulsar IGR J17480−2446 in the globular cluster Terzan 5 (Linares et al. 2012). We note that this object showed different behavior in its mHz oscillations compared to the others. During its outburst in 2011, as the flux increased, the recurrence time of bursts steadily decreased to about 3 minutes, finally appearing as oscillations in the light curve with this period. These oscillations also appeared at a much higher inferred accretion rate than in the other mHz sources (Linares et al. 2012; Galloway & Keek 2017).

Yu & van der Klis (2002) found that the frequency of kilohertz QPOs are anti-correlated with the brightness of the mHz oscillations in 4U 1608−52, and because this relationship is opposite to the positive correlation of kHz QPO frequency with X-ray luminosity typically seen, argued that the flux variation associated with the mHz QPO must arise on the neutron star surface and not within the accretion flow.

[1] https://personal.sron.nl/~jeanz/bursterlist.html

Altamirano et al. (2008) reported on extensive *Rossi X-ray Timing Explorer* (*RXTE*) observations of 4U 1636−536 that revealed a close connection between the mHz oscillations and the occurrence of X-ray bursts. They found that, during intervals of mHz oscillations, as the frequency drifted down and dropped below about 7.5 mHz, the oscillations faded and X-ray bursting resumed, and, similarly to Revnivtsev et al. (2001), they found no mHz oscillations immediately following the X-ray bursts.

More recently, Lyu et al. (2015) also studied episodes of mHz QPOs in 4U 1636−536 using *XMM-Newton* and *RXTE* data. Similarly to Altamirano et al. (2008), they found frequency drift of the mHz oscillations, and suggested the drift time-scale may be set by cooling of the deeper layers, as was previously argued by Keek et al. (2009) based on hydrodynamic calculations of helium burning with rotational mixing. Lyu et al. (2016) found that the bursts that occurred immediately after an episode of mHz oscillations preferentially showed a rising light curve shape with so-called positive "convexity." Such bursts show fast rise times, and this has been linked to a burst ignition location at or near the star's rotational equator (Maurer & Watts 2008; Cooper & Narayan 2007). Thus, Lyu et al. (2016) argued that these bursts, and the burning responsible for the mHz QPOs, may occur at the neutron star equator. Stiele et al. (2016) reported results from phase-resolved spectroscopy of the mHz oscillations in 4U 1636−536 obtained with *XMM-Newton*. They found an approximately constant color temperature with pulse phase of ≈ 0.7 keV that they associated with the neutron star surface, and argued that the oscillations result from a variation in the surface emitting area and not the temperature. They derived a surface emitting area consistent with that expected for a neutron star.

The physics relevant to marginally stable burning was recognized early on by Paczynski (1983), and has been further elucidated by Heger et al. (2007b). As the helium burning stability boundary is approached, the temperature dependence of the nuclear heating rate almost precisely balances that of the cooling rate. The result is a slow, quasiperiodic mode of burning, with the oscillation period given approximately by the geometric mean of the accretion and thermal time-scales. For typical neutron star parameters and the relevant accretion rates, this gives an oscillation period close to 2 min, which is in good agreement with the range of oscillation frequencies reported for the mHz oscillations.

Theory predicts that for unstable burning associated with helium ignition, the boundary between stable and unstable burning should occur at local accretion rates close to the Eddington rate (Bildsten 1998). The fact that observational indications based on estimates of the X-ray luminosity suggest the onset of stability at accretion rates closer to $\approx 1/10$ of the Eddington rate remains a major puzzle (van Paradijs et al. 1988; Cornelisse et al. 2003). It has been suggested that confinement of the accreted fuel, and/or rotational mixing of the fuel to greater column depths could alleviate this apparent discrepancy (Keek et al. 2009). The fact that the mHz oscillations associated with marginal stability occur at a well defined local ac-

cretion rate makes them, in principle, a particularly important probe of the accretion rate. Keek et al. (2014) found that the range of accretion rates in which marginally stable oscillations can occur was also sensitive to the nuclear reaction rates. Moreover, Heger et al. (2007b) showed that the oscillation frequency associated with marginal stability is sensitive to the hydrogen mass fraction in the accreted fuel, as well as the surface gravity. Thus, a more detailed understanding of these oscillations could lead to new probes of these quantities.

The accreting neutron star binary GS 1826−238 (hereafter, GS 1826) is in many ways a prototype, having earned the moniker "clocked burster," for producing bursts with extreme regularity (Ubertini et al. 1999). The recurrence times of these regular bursts were shown to match well the predictions of theory for mixed H/He bursts (Galloway et al. 2004), and the light curve shapes were accurately modeled using theoretical calculations of rapid-proton (rp)-process burning of approximately solar composition fuel (Heger et al. 2007a), hence, it has also been referred to as the "text-book" burster. Indeed, the bursts were so uniform in their properties that Zamfir et al. (2012) used them as "standard candles" to place constraints on the mass and radius of the neutron star.

The "clocked" bursts all occurred, however, while GS 1826 was in a "hard" spectral state. This is typically diagnosed with the use of X-ray colors (van der Klis 2006). Based on this, GS 1826 is classified as an "atoll" source, and the hard state is also referred to as the "island" state. Interestingly, Chenevez et al. (2016) recently reported on observations of GS 1826 in 2014 June with *Swift* and *NuSTAR* during a soft spectral state, including the detection of several X-ray bursts. They found that in this spectral state the X-ray burst recurrence times were no longer regular, and the bursts themselves also differed from the hard state bursts, being generally shorter in duration. These findings are indicative of a lower hydrogen fraction in the fuel, and suggest an additional source of stable burning occurs at the higher accretion rates in the soft state. They also detected the first photospheric radius expansion (PRE) burst from GS 1826, and used it to estimate the distance as 5.7 ± 0.2 kpc (assuming isotropic emission). Since then, the source has mostly remained in a soft state.

In this paper we report the discovery with *NICER* of mHz oscillations from GS 1826 that are very likely associated with marginally stable burning. The plan of the paper is as follows. We begin with a description of the observations and present the detection of mHz oscillations, and an X-ray burst. Next, we explore the source accretion state by studying the X-ray colors, showing that the source was in a soft, "banana" state in the color - color diagram (Hasinger & van der Klis 1989). Next we study the average mHz pulse profile, and present the results of phase-resolved spectroscopy. We conclude with a brief summary and discussion of the implications of our findings for models of marginally stable burning and for constraining the neutron star properties of GS 1826.

2. NICER OBSERVATIONS

NICER was installed on the International Space Station (*ISS*) in 2017 June, and provides low background, high throughput ($\approx$ 1900 cm^2 at 1.5 keV), fast timing observations across the $0.2 - 12$ keV X-ray band (Gendreau et al. 2012). *NICER* achieves an absolute timing precision of $\approx$ 100 ns with the aid of a GPS receiver. *NICER* observed GS 1826 as part of a science team program with a major goal to detect and study X-ray bursts. Observations were obtained in the periods 2017 June 20 - 29, July 11 - 13 and September 9 - 15. Relevant "observation IDs" (obsids) include 00503101nn and 10503101mm, where nn runs from 01 to 14 and mm from 01 to 16. We used HEASOFT version 6.23 and NICERDAS version 2018-03-01_V003 to process the data, and we applied the standard filtering criteria, which includes time intervals with a pointing offset $< 0.015°$ [2], bright Earth limb angles $> 40°$, dark Earth limb angles $> 30°$, and outside the South Atlantic Anomaly (SAA). This resulted in a total good exposure of 18, 6 and 10 ks for the June, July, and September epochs, respectively.

2.1. *mHz QPOs and an X-ray Burst*

We found that a few data intervals showed enhanced backgrounds at energies above ≈ 8 keV, so to mitigate this we restricted the timing analysis to events with energies less than 7.5 keV. We note that, because the observed count rate is decreasing with energy, only $\approx 0.5\%$ of all observed events have energies greater than this limit. We computed light curves for each epoch using events in the range $0.4 - 7.5$ keV. Figure 1 shows the resulting light curve, where the time axis is broken up into three panels, one each for the June, July, and September exposures, respectively. We identified a thermonuclear X-ray burst that occurred on 2017 June 22 at 22:31:42 UTC (labelled in Figure 1). The burst shows a hardness ratio evolution consistent with photospheric radius expansion (PRE), and also shows a shorter-duration light curve that differs from those of the hard state, "clocked" bursts (Galloway et al. 2004; Heger et al. 2007a), but is similar to bursts recently observed from GS 1826 in a high (soft) spectral state (Chenevez et al. 2016). We note that the publicly available data from the *Monitor of All-sky X-ray Image* (*MAXI*) and the *Swift Burst Alert Telescope* (*BAT*), are consistent with GS 1826 being predominantly in a soft spectral state from about 2016 December to the present. We will present a detailed spectral study of this burst in a subsequent paper.

Visual inspection of the light curves from the first two dwells of the September data epoch (these dwells are the first in the right-most panel of Figure 1, and are also labelled "mHz QPO") suggested the presence of apparent pulsations with a few minute period. The light curves of these dwells in the $0.4 - 7.5$ keV band, binned

[2] We note that obsids $0050310101 - 05$, inclusive, were obtained with an offset pointing of $0.03°$, which nominally violates the standard filtering criterion. However, this offset simply reduces the count rate modestly but does not otherwise effect our results, so we included these data in our analysis.

at 10 s, are shown in Figure 2. Pulses are rather clearly evident "by eye." To explore this apparent variability more quantitatively we computed power spectra using continuous intervals of 2200 s for each of these dwells. We again used events in the $0.4 - 7.5$ keV band, and sampled the light curves at 8192 Hz. The resulting power spectra, normalized as in Leahy et al. (1983), are shown in Figure 3, where the black and red curves correspond to the first and second dwells, respectively. Both spectra show strong, narrow peaks near 8 mHz, a frequency consistent with the few minute separation of pulses evident in Figure 2. These peaks are highly significant, for pure Poisson noise the chance probability to exceed a power value of 200 is 3.7×10^{-44}. From the power spectra shown in Figure 3 we estimate fractional amplitudes (rms) in the $0.4 - 7.5$ keV band for the first and second dwells of 0.79% and 0.95%, respectively. These values for the frequency and amplitude are largely consistent with those previously reported for mHz oscillations in other sources (Revnivtsev et al. 2001).

The mHz signal power from the first dwell is confined to a single Fourier bin, being effectively coherent over the length of the interval. The Fourier frequency of this bin is 8.18 mHz. In the second dwell the peak power shifts down one Fourier bin, and significant power is spread over a few bins. This suggests a downward drift in the oscillation frequency from the first to second dwell. To quantify this drift we oversampled the power spectrum for each dwell by padding the light curve to 8000 s using the mean count rate determined from the good exposure (2200 s). We then found the mHz frequency associated with the peak power in each spectrum. From the frequency separation, $\Delta\nu$, of the peak power values we estimate a frequency drift rate of $\Delta\nu/\Delta t \approx -0.3$ mHz hr^{-1}. Previous studies of mHz oscillations indicate that the frequency can both increase and decrease with time, and that the frequency drift rate can vary (Lyu et al. 2014, 2015; Altamirano et al. 2008). The best-studied object in this regard is 4U 1636−536. The rate of decrease we estimate here for GS 1826 does not appear to be inconsistent with previous reports (Altamirano et al. 2008), that is, one can find time intervals reported in the literature for 4U 1636−536 which have approximately similar drift rates (see, for example, Figure 4 in Lyu et al 2015).

After identifying the strong mHz pulsations described above, we also searched for similar signals in the remaining data. We note that many of the other individual dwells have exposures that are shorter than those of the 2017 September dwells with strong mHz oscillations. So, not all observations are equally sensitive to such oscillations. Nevertheless, we searched for additional signals by computing power spectra of all dwells with exposures equal to or longer than 750 s ($0.4-7.5$ keV band). We detected mHz oscillation signals near 8 mHz in three other dwells, while for the remainder no signal was detected, and we obtain upper limits (90% confidence) to an oscillation in the 7 - 9 mHz frequency band that range from approximately $0.3 - 0.5$% (rms), with the precise value depending on the count rate and exposure of the particular dwell. Figure 4 shows power spectra from these three additional dwells with mHz

oscillations. The spectra are labelled with the start date (MJD) of the dwell, and the number in parenthesis indicates the corresponding day in Figure 1. The successive spectra are displaced vertically by 100 for clarity. From figure bottom to top we estimate fractional amplitudes (rms) of 0.60, 0.85 and 0.65%. We also searched for mHz oscillations in the immediate aftermath of the X-ray burst detected on 2017 June 22, but no mHz signal was detected in a power spectrum computed from a 600 s interval ($0.4-7.5$ keV) following the burst. The upper limit on the amplitude is 0.5% (rms). Finally, we did not detect mHz oscillations in any of the dwells preceding the X-ray burst.

2.2. *Spectral State*

To further explore the accretion state context of the mHz oscillations we calculated color - color and hardness - intensity diagrams for all the data. We computed both a "soft" and "hard" color. For the former we determine the ratio of count rates in the bands $1.8-3.5$ and $0.5-1.8$ keV, while for the latter we use $5.2-6.8$ and $3.5-5.2$ keV. For the intensity we compute the count rate from $0.5-6.8$ keV. We computed colors and intensities using 32 s intervals for all the data. Figures 5 and 6 show the resulting color - color, and hardness - intensity diagrams, respectively. In both figures the blue (triangle) symbols represent data obtained from the two September epoch intervals when strong mHz oscillations were present, and the red (diamond) symbols were obtained from intervals immediately following the X-ray burst. A characteristic error bar is also shown in each plot to indicate the statistical precision.

To further elucidate the relationship between the spectral colors and mHz oscillations we computed colors for all dwells in which oscillations were detected, as well as some of the longer dwells with no detections, and only upper limits. The colors measured for all of these dwells are shown in Figure 7, where the red diamond symbols represent those with upper limits, the blue square symbols those with mHz oscillation detections, and the size of the blue symbols is proportional to the oscillation amplitude (rms). The X-ray colors are defined in the same way as in Figure 5. These results suggest that the presence and amplitude of mHz oscillations is related to position in the color - color diagram, and therefore the mass accretion rate, as dwells with the highest amplitudes seem to occur preferentially at the higher values of soft and hard color. Such behavior is theoretically predicted for mHz oscillations associated with marginally stable burning (Heger et al. 2007b), as they are only evident close to the mass accretion rate at which burning stabilizes. It may be that we are seeing such a transition in Figure 7, since mHz oscillations are not detected at the lowest inferred accretion rates (the lower left portion of the color - color diagram). However, it is also possible that this behavior is similar to that seen in 4U 1636−536, where mHz oscillations can "come and go" while on the "banana" branch (Altamirano et al. 2008). The present data are too sparse to be conclusive, and more observations will be needed to distinguish between these two possibilities.

3. PROPERTIES OF MHZ OSCILLATIONS

Since the power spectra (Figure 3) from the two 2017 September dwells with strong mHz oscillations are consistent with rather coherent oscillations during these intervals, we computed phases for all events in each of these dwells separately using the frequencies corresponding to the peak Fourier power obtained from each dwell. To combine the two dwells we first found a constant phase offset for the 2nd dwell that maximized the Z_1^2 signal power of the sum of both dwells (Buccheri et al. 1983). The resulting phase folded pulse profile in the $0.4-7.5$ keV band is shown in Figure 8. We fit a model of the form $A + B\sin(\phi - \phi_0)$ and find an amplitude $B/A = 1.12 \pm 0.05\%$. The fit is good with a minimum $\chi^2 = 11.0$ for 13 degrees of freedom, and the best fitting model is also plotted in Figure 8 (red curve). To explore the energy dependence we also computed profiles for different energy bands and then fit them with the same model as above. Figure 9 shows the derived amplitudes, B/A, and phases, ϕ_0, versus energy. The amplitude shows a modest increase from about 0.7% at 1 keV to $\approx 2\%$ at 7 keV. There is no strong evidence for a variation in ϕ_0 with energy.

To explore the pulse-phase spectrum we extracted two spectra, from regions around the pulse minimum and maximum. The phase ranges used for these extractions are indicated by the dashed and dash-dotted vertical lines in Figure 8, respectively. In each case we used a range of pulse phase equal to 0.25 cycles, so that each spectrum has an exposure of $0.25 \times (2(2200)) = 1100$ s. We used XSPEC version 12.9.1 with version 1.02 of the *NICER* instrument response, and we fit the spectra in the range $0.6-9$ keV. We use a model comprised of thermal comptonization (*comptt* in XSPEC) for the persistent accretion-driven emission and a black body (*bbodyrad* in XSPEC) to capture the neutron star thermal emission (Chenevez et al. 2016; Thompson et al. 2008). To model Galactic absorption we employ the *tbabs* model with abundances from Wilms et al. (2000), and we fix (freeze) the value of $n_H = 0.4 \times 10^{22}$ cm^{-2} based on prior measurements, since the source is in the same (soft) state (Chenevez et al. 2016; Pinto et al. 2010). We employ a background spectrum extracted from *NICER* observations of *RXTE* background field number 5 (Jahoda et al. 2006), but we note that the spectrum is strongly source dominated across the fitted band. Finally, we add a 1% systematic error to accommodate current uncertainties in the *NICER* response.

As with many X-ray spectral modeling efforts, there is often no single, unique approach. The same is true in this case. In order to model either individual phase-resolved spectrum we find that both of the spectral components discussed above are required. However, the data do not have sufficient statistical quality to simultaneously fit for all parameters and determine unambiguously whether either of the components alone is associated with the mHz modulation. That is, one can either fix the persistent component (*comptt*) to be the same between the phase maximum and minimum spectra, or one can fix the black body (*bbodyrad*) component. Given the statistical quality of the present spectra one can achieve a similarly good fit using either approach. Below, we explore the approach that the persistent emission is not

Table 1. Phase-resolved spectral fits for GS 1826

Component	Parameter	Spectrum minimum	Spectrum maximum
tbabs	n_H (10^{22} cm^{-2})	0.4	tied
compTT	kT_0 (keV)	0.095 ± 0.014	tied
	kT_e (keV)	2.03 ± 0.04	tied
	τ	8.4 ± 0.1	tied
	norm	1.88 ± 0.20	tied
bbodyrad	kT (keV)	0.684 ± 0.006	0.701 ± 0.005
	K (*norm*)	603.7 ± 14.3	599.0 ± 13.1

Note—Parameter uncertainties are given at 1σ confidence, and those with no quoted uncertainty were held fixed at the indicated value.

strongly affected by the mHz oscillation, and assume that the difference between the two spectra is accounted for by the black body component. This appears reasonable given the modest $1-2\%$ amplitude of the modulation, and the theoretical suggestion that such oscillations arise from the neutron star surface. However, we emphasize that this approach places constraints on the black body component *under the assumption that it is the varying component*, but it does not demonstrate unambiguously that it is the varying component.

Thus, we carry out a joint fit to both the minimum and maximum phase spectra, keeping the *comptt* parameters and the column depth, n_H, tied together, but allowing the black body parameters to vary independently between the two spectra.

We find this model provides a reasonable description of the observed spectra, with a reduced $\chi^2_r \approx 1.01$ ($\chi^2 = 1698$ with 1676 degrees of freedom). The largest remaining residuals are centered near 2.3 keV, and this feature is associated with a known instrumental edge (see Ludlam et al. (2018) for further discussion of the *NICER* spectral response). Our spectral results are summarized in Table 1. Figure 10 shows the unfolded, photon spectra, including the individual model components (top), and the fit residuals (bottom). The mean (unabsorbed) flux in the 0.6 - 9 keV band is $6.90 \pm 0.01 \times 10^{-9}$ erg cm^{-2} s^{-1}. For the comptonization component parameters we find results that are qualitatively similar to Chenevez et al. (2016), but differ somewhat in the details. For the black body components we find that the fitted normalizations are consistent with remaining constant from pulse minimum to maximum, with a mean value of $K_{avg} = 601.3$. This normalization corresponds to an area, assuming a spherical emitting source and isotropic emission, with radius $R = (K_{avg} d_{10}^2)^{1/2} = 13.98$ km, where d_{10} is the distance in units of 10 kpc, and we have assumed $d = 5.7$ kpc (Chenevez et al. 2016). We note that this estimate ignores any atmospheric color corrections. Applying such a correction would increase the inferred radius by a factor of $f_c^2 = (T_c/T_{eff})^2$, where T_c and T_{eff} are the color (measured) and effective temperatures, respectively, and f_c is the so-called hardening

factor. Based on model atmosphere calculations, f_c is likely to fall within the range from $\approx 1.2 - 1.5$ (Medin et al. 2016; Suleimanov et al. 2011), resulting in an increase in inferred radius by a factor of $\approx 1.4 - 2.2$. However, given the other assumptions and uncertainties, the value is at least approximately consistent with expectations for surface emission from a neutron star.

For the spectra at maximum and minimum oscillation phase we find temperature values of $kT = 0.701 \pm 0.005$ keV, and $kT = 0.684 \pm 0.006$ (both 1σ confidence), respectively. This suggests that the flux modulation associated with the mHz oscillation appears to be consistent with a change in the surface temperature, kT, of the neutron star thermal emission. However, we note that these values differ only at the $\approx 3\sigma$ level, and more data are needed to demonstrate this conclusively.

4. DISCUSSION

We report the detection with *NICER* of mHz oscillations in GS 1826 for the first time. The oscillation properties are generally consistent with those of the mHz QPOs observed in 4U 1608−52, 4U 1636−536, Aql X-1, and 4U 1323−619. The *NICER* data were obtained while GS 1826 was in a soft spectral state, as indicated by both *MAXI* (Sugizaki et al. 2011) and *Swift/BAT* (Krimm et al. 2013) long-term monitoring from about 2015 December to the present. Indeed, the current long-term trend appears to be a slow but steady increase in the 2 - 10 keV flux (based on the *MAXI* data), and very weak hard X-ray flux (from *Swift*-BAT). Our spectral color analysis appears consistent with this conclusion as well. The observed behavior (Figures 5, 6 and 7) appears consistent with GS 1826 tracing out a portion of the so-called "banana" branch in the color - intensity diagram during the *NICER* observations. The mass accretion rate is generally inferred to increase from left to right along the arc of the "banana." To further test this we extracted spectra from several intervals which populate the lower left portion of the color - color diagram (see Figure 7), in order to estimate their fluxes and compare with the mean flux measured during the September epoch intervals with strong mHz oscillations (see §2.2 above). We find these spectra can be fit with the same model described above, and we find the unabsorbed flux (0.6 - 9 keV) in the range from $5.0 - 5.2 \times 10^{-9}$ erg cm^{-2} s^{-1}, supporting the conclusion that the X-ray flux, and therefore mass accretion rate, increases from lower left to upper right in the color - color diagram (Figure 7).

Assuming the X-ray luminosity can be written as,

$$L_x = \frac{GM\dot{M}}{(1+z)R} = 4\pi d^2 f_x \ , \tag{1}$$

where M, R, $(1+z) = (1-2GM/c^2R)^{-1/2}$, and f_x are the neutron star mass, radius, surface redshift, and X-ray flux respectively, we estimate an average mass accretion rate, $\dot{M}$, for the September dwells with mHz oscillations of $\dot{M} = 0.18\dot{M}_{Edd}$, where we have assumed $M = 1.4M_\odot$, $R = 10$ km, $d = 5.7$ kpc, and $\dot{M}_{Edd} = 1.7 \times 10^{-8} M_\odot$ yr^{-1}. This estimate also assumes that the accretion luminosity is radiated isotropically.

Previous studies have shown that mHz oscillations can be associated with bursting activity. For example, Altamirano et al. (2008) found episodes of mHz oscillations in 4U 1636−536 with decreasing frequency, and when the frequency dropped below about 7.5 mHz the oscillations faded and bursting resumed; however, such behavior was not associated with *all* X-ray bursts (see their Figure 3). Indeed, the data for 4U 1636−536 suggest that intervals of mHz oscillations can come and go without an obvious trigger, as long as the source is in the appropriate accretion state, indicated by its position on the banana branch or in the transition to the banana branch (see Altamirano et al. 2008, Figure 1). For GS 1826 we find no evidence for mHz oscillations after the X-ray burst on 22 June, which at face value is consistent with the behavior seen in 4U 1636−536. However, we emphasize that the present data are very sparse around the time of the X-ray burst. The only thing we can say with certainty is that we did not detect mHz oscillations in any of the *NICER* dwells preceeding the X-ray burst or immediately after it.

Our results suggest the following long term behavior in GS 1826. Prior to 2014 the source was almost exclusively in the hard state, with typical accretion rates lower than indicated by the present *NICER* observations. For example, comparing long term variations in the persistent X-ray flux–a reasonable proxy for mass accretion rate–we find from Galloway et al. (2004) that the $2.5-25$ keV persistent (absorbed) flux from *RXTE* observations was 2.2×10^{-9} erg cm^{-2} s^{-1} on July 29, 2002. Based on the *NICER* spectral modeling for the 2017 September epochs described above we estimate a flux in the same band of 4.5×10^{-9} erg cm^{-2} s^{-1}, a factor of two or so higher. In making this estimate we note that we have extrapolated the best-fit *NICER* model (Table 1) to 25 keV, that is, outside of *NICER*'s nominal bandpass. However, the (absorbed) flux measured by *NICER* in the $2.5-9$ keV band is 3.6×10^{-9} erg cm^{-2} s^{-1}, which is already significantly larger than the 2.5−25 keV *RXTE* flux. Since the $2.5-9$ keV *NICER* flux measurement is a firm lower bound to the $2.5-25$ keV flux, this strongly suggests that the flux measured by *NICER* in 2017 September *in the same band* is significantly higher than the July 2002 flux measured with *RXTE*. This provides further support to the notion that the apparent long-term increase in X-ray flux likely represents an increasing mass accretion rate.

While in the hard state the source was extensively observed with *RXTE*, but no mHz QPOs were ever observed. As the source continued to brighten and soften, the accretion rate became large enough to enter the accretion regime where mHz oscillations are observed in other LMXBs (see, for example, Altamirano et al. 2008, Figure 1). This overall behavior appears consistent with the observations of the mHz QPOs in 4U 1636−536, 4U 1608−52 and Aql X-1, and suggests we are seeing the same phenomenon in GS 1826. More observations of GS 1826 in its soft, higher accretion rate state will be needed to determine if it shows the full range of mHz oscillation phenomenology evident in other sources, including a closer connection with X-ray bursts.

There have been some reports of QPOs not linked with marginally stable burning, but with similar frequencies. In some of those cases the accretor is known or strongly suspected to be a black hole and not a neutron star. Examples are the QPOs identified in the black hole candidates H1743−322 (Altamirano & Strohmayer 2012), and LMC X-1 (Alam et al. 2014). In the case of H1743−322, the QPOs are seen in a hard spectral state, whereas the mHz QPOs reported here occur in the soft state of GS 1826. For LMC X-1 the observed QPO frequencies are higher, at ≈ 27 mHz, than any previously reported mHz oscillation associated with marginally stable burning. Based on this it appears unlikey to us that the mHz oscillations observed in GS 1826 are related to these QPOs.

Several accreting millisecond X-ray pulsars have also occasionally shown episodes of QPOs with mHz frequencies during some outbursts, an example being the 8 mHz "flaring" observed in IGR J00291+5934 (Ferrigno et al. 2017). In those QPOs, however, the modulation amplitude was $> 10\%$ (rms) for photon energies less than 2 keV, which is substantially larger than is found for the mHz oscillations linked to marginally stable burning. Morever, the energy spectrum softened at the peak of these flares, which is opposite to the behavior indicated in GS 1826. This argues rather strongly that the mHz oscillations reported here from GS 1826 are not related to these mHz "flaring" QPOs.

As discussed in §2.1 the oscillations reported here from GS 1826 have a rather high quality factor, that is, they appear to be rather coherent over the intervals they are observed. We emphasize, however, that these intervals (≈ 2 ks) are relatively short compared to the hours-long time-scales over which mHz QPO frequencies have been observed to drift in several sources (Lyu et al. 2015; Altamirano et al. 2008). Additionally, current modeling of marginally stable burning can produce quite regular trains of mHz pulses, with the limiting factor here likely being temporal variations of the mass accretion rate (Heger et al. 2007b; Keek et al. 2014). Based on these arguments we think that the relatively high coherence seen in the mHz oscillations reported here is not inconsistent with their connection to marginally stable burning.

Figure 9 shows the energy dependence of the fractional (sinusoidal) modulation amplitude of the mHz oscillations in GS 1826. From about $1 - 3$ keV an increasing trend is rather clear, with an apparent flattening above 3 keV. This appears to be at least qualitatively similar to the behavior seen in IGR J17480−2446–which shows an increasing trend in rms amplitude from about $2.5 - 10$ keV based on *RXTE* data (Linares et al. 2012)–but opposite to that reported for 4U 1608−52 and 4U 1636−536 by Revnivtsev et al. (2001), also using *RXTE*. However, some caution is warranted here due to the different bandpasses of *NICER* and *RXTE*, as well as the extent to which uncertainties in backgrounds could influence derived amplitudes. A closer comparison of the energy dependence of the mHz oscillations reported here with *NICER*, and those detected with *XMM-Newton* should prove useful, as these instruments have more closely matched bandpasses.

We extracted spectra as a function of mHz pulsation phase, and find that they are consistent with the modulation being produced by a variation in the temperature of a thermal (black body) component at an effectively constant emitting area, though we emphasize again that this is not a unique spectral interpretation (see discussion in §3 above). Assuming a spherical emitting source and isotropic emission, the fitted black body normalization implies a radius of $R \approx 14$ km. Given uncertainties in the source distance, the exact nature of the continuum describing the persistent emission, the extent to which disk reprocessing is present, as well as our neglect of color corrections, this value should only be taken as roughly indicative of the surface area associated with the mHz oscillations, and definitely not a precise measurement. The evidence that the oscillating flux can be associated with a thermal (black body) component with an area approximately consistent with that for a neutron star provides support for the interpretation of the oscillations as due to marginally stable nuclear burning; however, more data will be needed to establish this definitively.

We note that Stiele et al. (2016) reached different conclusions from a study of the phase-resolved spectra of mHz oscillations from 4U 1636−536. They argued that the flux modulation resulted from a variation in the emitting area at approximately constant temperature. While this is at odds with current theory, which finds that the temperature oscillates (Heger et al. 2007b), we emphasize that current theoretical calculations of marginally stable burning are all one dimensional, so they essentially do not explore the possibility of variations in the burning area.

Here we point out that there are several physical effects that suggest that lateral variations in the burning should be included in future modeling. For example, Heger et al. (2007b) showed that the oscillations associated with marginal stability occur in a very narrow range of mass accretion rates, $\dot{m}$, for a given surface gravity. They found the oscillations were present in a range of only 1% of the critical accretion rate. Note that it is the *local* accretion rate that is relevant for the nuclear burning. For a fast spinning neutron star the variations in effective surface gravity from equator to pole can result in a latitudinal change in the local accretion rate. Cooper & Narayan (2007) used this effect to explore the extent to which ignition of thermonuclear bursts could preferentially occur at different latitudes. However, this process would appear to be relevant for marginally stable burning as well, as a greater than 1% variation in the local accretion rate with latitude could influence the range of stellar latitudes for which marginally stable oscillations could occur. Indeed, this appears to be a possible mechanism for limiting the marginally stable burning to a belt in latitude (Lyu et al. 2016). As a rough guide, a star rotating at 582 Hz (close to the inferred spin frequency for 4U 1636−536), and with a mass of $1.4 M_\odot$ and equatorial radius of 10 km, would have an $\approx 11\%$ increase in effective surface gravity from equator to pole, using the results of AlGendy & Morsink (2014). This is certainly large enough to have a significant effect on the local accretion rate at the level required to influence marginally stable burning. Interestingly, for a spin rate

of 11 Hz, appropriate for IGR J17480−2446 in Terzan 5, the variations in surface gravity are $< 0.004\%$ equator to pole, and thus latitudinal variations would likely be negligible for such a slow spinner. This could perhaps account for some of the observed differences in the mHz oscillations of IGR J17480−2446 and fast spinners like 4U 1608−52, 4U 1636−536, and Aql X-1. As pointed out by Heger et al. (2007b), the critical accretion rate for marginally stable oscillations is itself a function of surface gravity, so the occurrence of oscillations, and their properties, will in principle depend on both effects; however, this discussion highlights that such latitudinal dependencies of the burning are likely, at least for fast spinners, and should be considered in future modeling of marginally stable oscillations.

Heger et al. (2007b) argued that the oscillation frequency associated with marginally stable burning should be sensitive to the neutron star surface gravity, which is proportional to M/R^2, and the mass fraction of hydrogen in the accreted matter (see their Figure 9). While their results on this score were based on one-zone models, the good overall agreement between predictions of their one-zone models and multi-zone hydrodynamic calculations with the KEPLER code (Heger et al. 2007b), suggests that these dependencies are robust. This is particularly promising for GS 1826 because of the extensive theoretical modeling already done on the "clocked" bursts (Heger et al. 2007a; Meisel 2018), which suggests a near solar composition for the accreted fuel. Interestingly, the bursts observed so far at the higher accretion rates associated with the soft spectral state have shorter durations, and several have reached higher peak fluxes, as is evidenced by the occurrence of PRE. These are both good indications of depletion of hydrogen in the fuel compared to the hard-state, "clocked" bursts. This suggests that additional theoretical modeling of the soft state bursts, coupled with further comparisons to the "clocked" bursts, could place tighter constraints on the hydrogen fraction present in the fuel during episodes of mHz oscillations. It might then be possible to provide more robust limits on the neutron star surface gravity from measurements of the mHz oscillations.

This work was supported by NASA through the *NICER* mission and the Astrophysics Explorers Program. This research also made use of data and/or software provided by the High Energy Astrophysics Science Archive Research Center (HEASARC), which is a service of the Astrophysics Science Division at NASA/GSFC and the High Energy Astrophysics Division of the Smithsonian Astrophysical Observatory. DA acknowledges support from the Royal Society. SG acknowledges the support of the Centre National d'Etudes Spatiales (CNES). We thank the anonymous referee for their efforts.

Facility: NICER, ADS, HEASARC

REFERENCES

Alam, M. S., Dewangan, G. C., Belloni, T., Mukherjee, D., & Jhingan, S. 2014, MNRAS, 445, 4259, doi: 10.1093/mnras/stu2048

AlGendy, M., & Morsink, S. M. 2014, ApJ, 791, 78, doi: 10.1088/0004-637X/791/2/78

Altamirano, D., & Strohmayer, T. 2012, ApJL, 754, L23, doi: 10.1088/2041-8205/754/2/L23
Altamirano, D., van der Klis, M., Wijnands, R., & Cumming, A. 2008, ApJL, 673, L35, doi: 10.1086/527355
Bildsten, L. 1998, in NATO Advanced Science Institutes (ASI) Series C, Vol. 515, NATO Advanced Science Institutes (ASI) Series C, ed. R. Buccheri, J. van Paradijs, & A. Alpar, 419
Buccheri, R., Bennett, K., Bignami, G. F., et al. 1983, A&A, 128, 245
Chenevez, J., Galloway, D. K., in 't Zand, J. J. M., et al. 2016, ApJ, 818, 135, doi: 10.3847/0004-637X/818/2/135
Cooper, R. L., & Narayan, R. 2007, ApJL, 657, L29, doi: 10.1086/513077
Cornelisse, R., in't Zand, J. J. M., Verbunt, F., et al. 2003, A&A, 405, 1033, doi: 10.1051/0004-6361:20030629
Cumming, A., & Bildsten, L. 2001, ApJL, 559, L127, doi: 10.1086/323937
Ferrigno, C., Bozzo, E., Sanna, A., et al. 2017, MNRAS, 466, 3450, doi: 10.1093/mnras/stw3344
Galloway, D. K., Cumming, A., Kuulkers, E., et al. 2004, ApJ, 601, 466, doi: 10.1086/380445
Galloway, D. K., & Keek, L. 2017, ArXiv e-prints. https://arxiv.org/abs/1712.06227
Gendreau, K. C., Arzoumanian, Z., & Okajima, T. 2012, in Proc. SPIE, Vol. 8443, Space Telescopes and Instrumentation 2012: Ultraviolet to Gamma Ray, 844313
Hasinger, G., & van der Klis, M. 1989, A&A, 225, 79
Heger, A., Cumming, A., Galloway, D. K., & Woosley, S. E. 2007a, ApJL, 671, L141, doi: 10.1086/525522
Heger, A., Cumming, A., & Woosley, S. E. 2007b, ApJ, 665, 1311, doi: 10.1086/517491
Jahoda, K., Markwardt, C. B., Radeva, Y., et al. 2006, ApJS, 163, 401, doi: 10.1086/500659
Keek, L., Cyburt, R. H., & Heger, A. 2014, ApJ, 787, 101, doi: 10.1088/0004-637X/787/2/101
Keek, L., Langer, N., & in't Zand, J. J. M. 2009, A&A, 502, 871, doi: 10.1051/0004-6361/200911619
Krimm, H. A., Holland, S. T., Corbet, R. H. D., et al. 2013, ApJS, 209, 14, doi: 10.1088/0067-0049/209/1/14
Leahy, D. A., Darbro, W., Elsner, R. F., et al. 1983, ApJ, 266, 160, doi: 10.1086/160766
Linares, M., Altamirano, D., Chakrabarty, D., Cumming, A., & Keek, L. 2012, ApJ, 748, 82, doi: 10.1088/0004-637X/748/2/82
Ludlam, R. M., Miller, J. M., Arzoumanian, Z., et al. 2018, ApJL, 858, L5, doi: 10.3847/2041-8213/aabee6
Lyu, M., Méndez, M., & Altamirano, D. 2014, MNRAS, 445, 3659, doi: 10.1093/mnras/stu1992
Lyu, M., Méndez, M., Altamirano, D., & Zhang, G. 2016, MNRAS, 463, 2358, doi: 10.1093/mnras/stw2158
Lyu, M., Méndez, M., Zhang, G., & Keek, L. 2015, MNRAS, 454, 541, doi: 10.1093/mnras/stv1971
Maurer, I., & Watts, A. L. 2008, MNRAS, 383, 387, doi: 10.1111/j.1365-2966.2007.12558.x
Medin, Z., von Steinkirch, M., Calder, A. C., et al. 2016, ApJ, 832, 102, doi: 10.3847/0004-637X/832/2/102
Meisel, Z. 2018, ApJ, 860, 147, doi: 10.3847/1538-4357/aac3d3
Paczynski, B. 1983, ApJ, 264, 282, doi: 10.1086/160596
Pinto, C., Kaastra, J. S., Costantini, E., & Verbunt, F. 2010, A&A, 521, A79, doi: 10.1051/0004-6361/201014836
Revnivtsev, M., Churazov, E., Gilfanov, M., & Sunyaev, R. 2001, A&A, 372, 138, doi: 10.1051/0004-6361:20010434
Stiele, H., Yu, W., & Kong, A. K. H. 2016, ApJ, 831, 34, doi: 10.3847/0004-637X/831/1/34

Strohmayer, T., & Bildsten, L. 2006, New views of thermonuclear bursts, ed. W. H. G. Lewin & M. van der Klis, 113–156

Strohmayer, T. E., & Altamirano, D. 2012, in American Astronomical Society Meeting Abstracts, Vol. 219, American Astronomical Society Meeting Abstracts #219, 249.03

Strohmayer, T. E., & Brown, E. F. 2002, ApJ, 566, 1045, doi: 10.1086/338337

Sugizaki, M., Mihara, T., Serino, M., et al. 2011, PASJ, 63, S635, doi: 10.1093/pasj/63.sp3.S635

Suleimanov, V., Poutanen, J., & Werner, K. 2011, A&A, 527, A139, doi: 10.1051/0004-6361/201015845

Thompson, T. W. J., Galloway, D. K., Rothschild, R. E., & Homer, L. 2008, ApJ, 681, 506, doi: 10.1086/588723

Ubertini, P., Bazzano, A., Cocchi, M., et al. 1999, ApJL, 514, L27, doi: 10.1086/311933

van der Klis, M. 2006, Rapid X-ray Variability, ed. W. H. G. Lewin & M. van der Klis, 39–112

van Paradijs, J., Penninx, W., & Lewin, W. H. G. 1988, MNRAS, 233, 437, doi: 10.1093/mnras/233.2.437

Wilms, J., Allen, A., & McCray, R. 2000, ApJ, 542, 914, doi: 10.1086/317016

Yu, W., & van der Klis, M. 2002, ApJL, 567, L67, doi: 10.1086/339771

Zamfir, M., Cumming, A., & Galloway, D. K. 2012, ApJ, 749, 69, doi: 10.1088/0004-637X/749/1/69

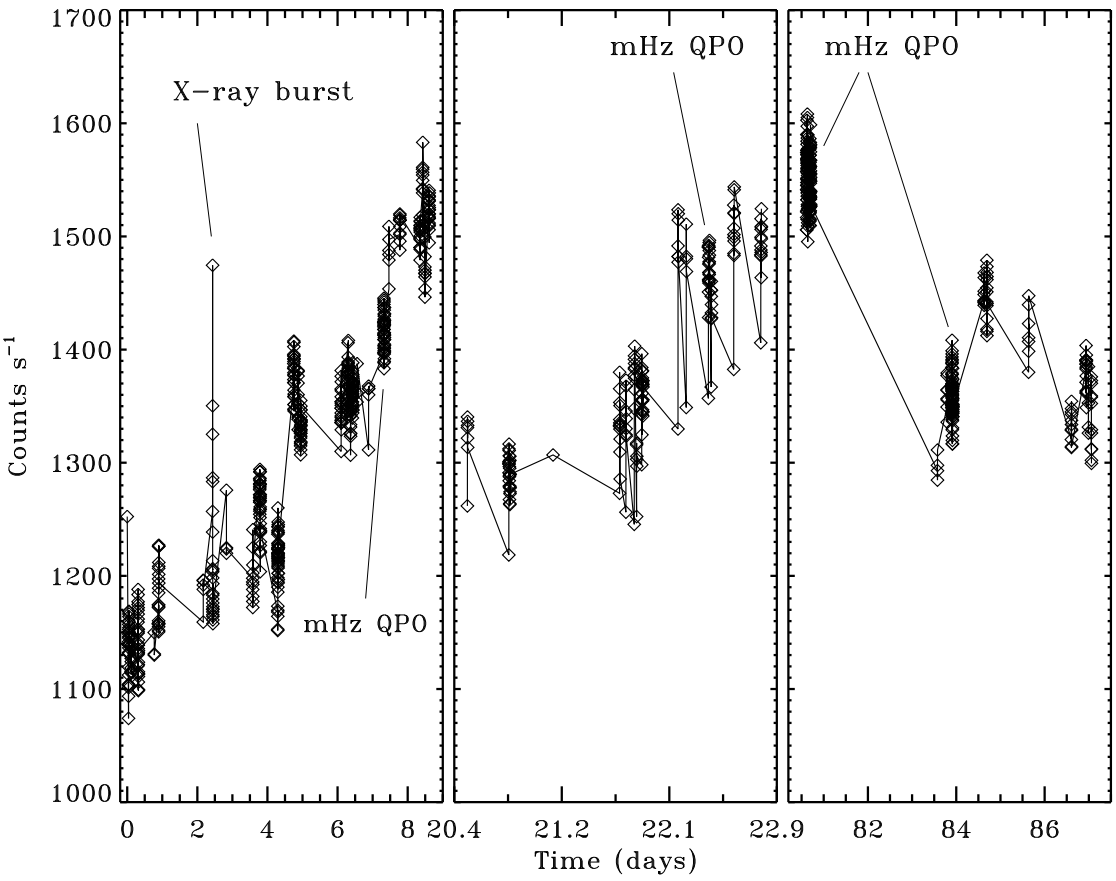


Figure 1. Light curve of GS 1826 from *NICER* observations obtained in 2017 June, July and September. Count rates are computed in 32 s bins including events in the 0.4 - 7.5 keV band. The time axis is broken up into three panels, one each for the June, July, and September exposures, respectively. Time zero corresponds to MJD 57924.54154 (TT). Intervals containing an X-ray burst and mHz oscillations are indicated.

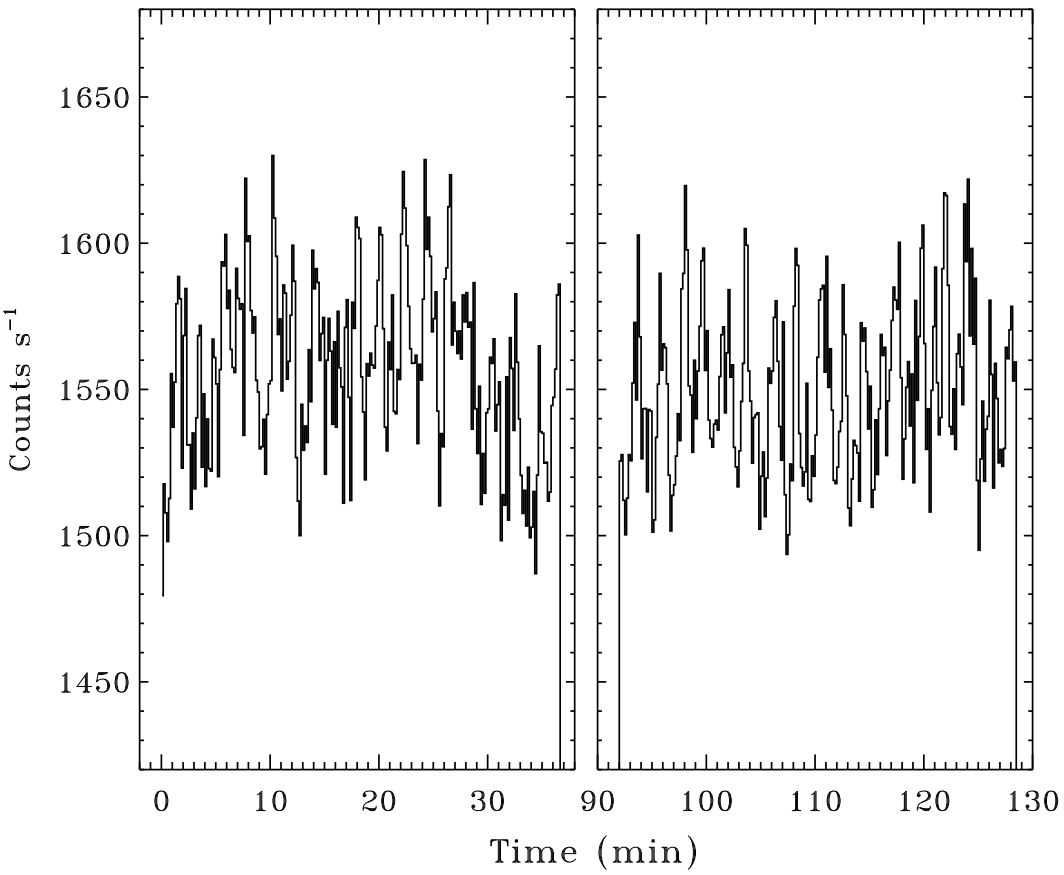


Figure 2. Light curves of GS 1826 from *NICER* observations over two consecutive *ISS* orbits on 2017 September 9. The count rates are computed in 10 s bins including events in the 0.4 - 7.5 keV band. Pulses with a period near 2 min can clearly be seen. Time zero corresponds to MJD 58005.11848988 (TT).

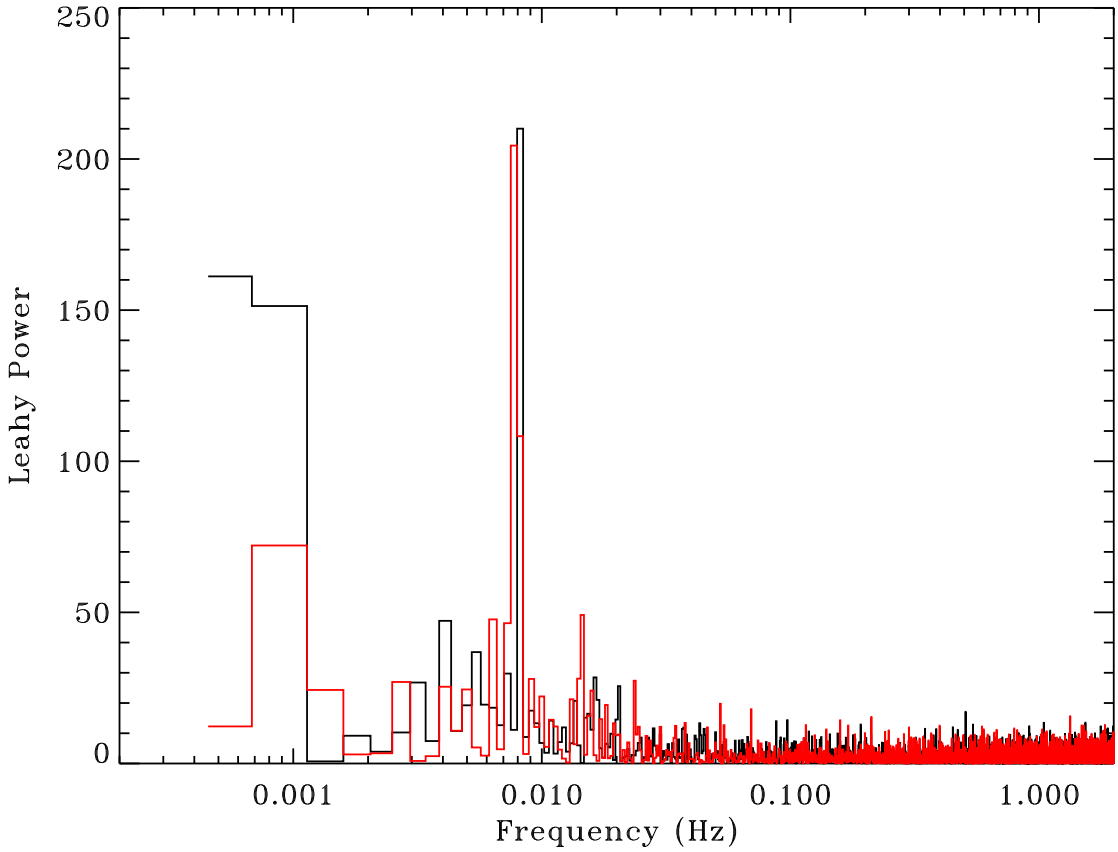


Figure 3. Power spectra of GS 1826 from the two *NICER* dwells shown in Figure 2. The black and red traces correspond to the spectra from the first and second dwells, respectively. Strong, narrow peaks are evident near 8 mHz from both dwells.

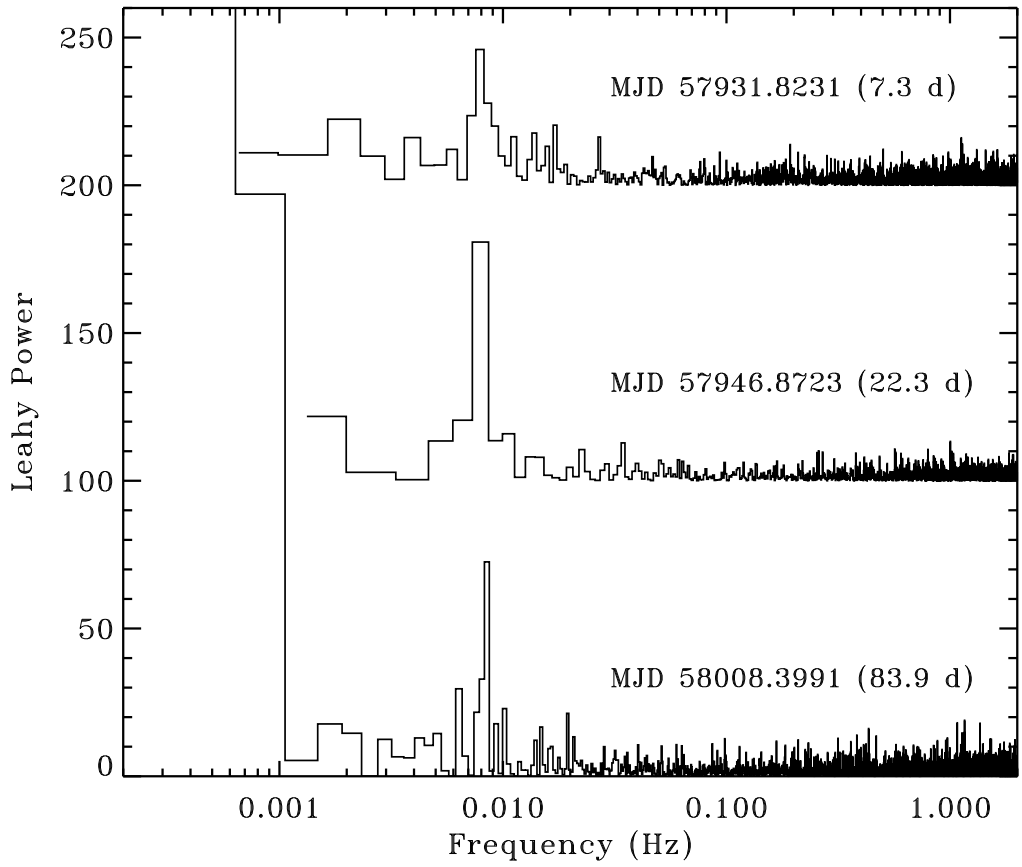


Figure 4. Power spectra of GS 1826 from three additional *NICER* dwells with mHz oscillations. As in Figure 2, significant peaks near 8 mHz are evident in each spectrum. Each spectrum is labelled with the start time (MJD) of the dwell, with the number in parenthesis indicating the corresponding time (day) in Figure 1. Each successive spectrum is displaced vertically by 100 for clarity.

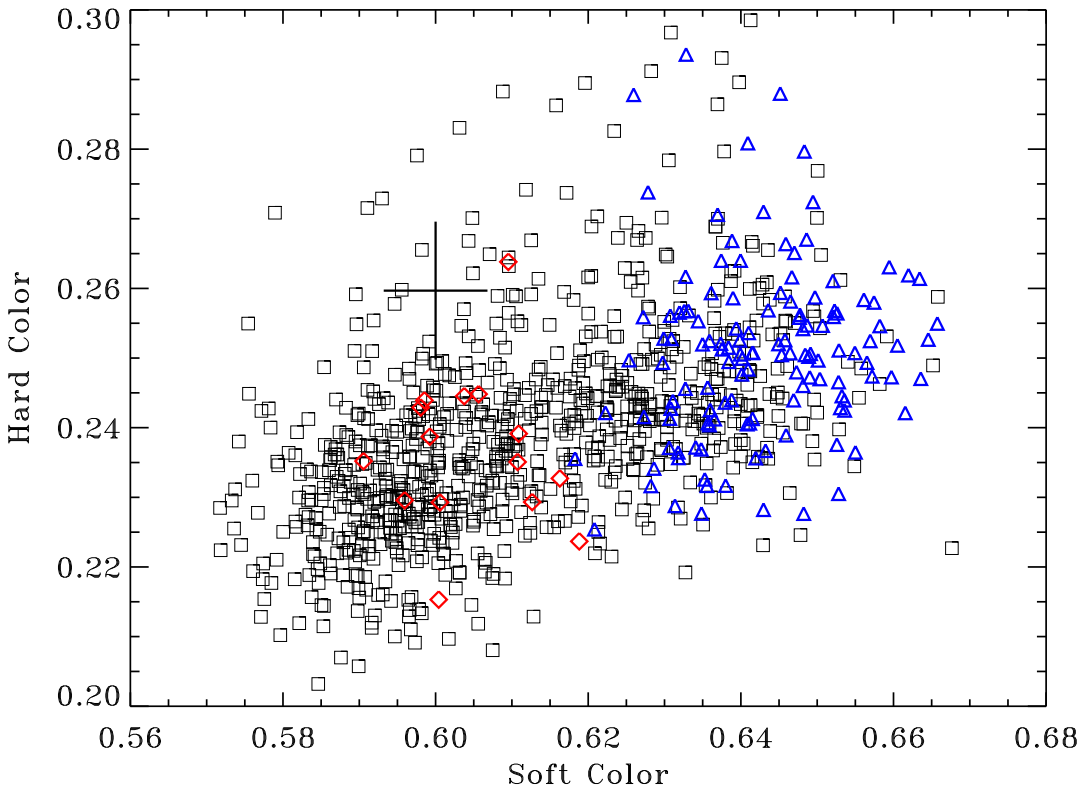


Figure 5. Color - color diagram of GS 1826 from 34 ks of *NICER* data obtained in the 2017 June, July and September epochs. The hard color is computed as the ratio of count rates in the $5.2 - 6.8$ and $3.5 - 5.2$ keV bands. For the soft color we used the $1.8 - 3.5$ and $0.5 - 1.8$ keV bands. Colors were computed using 32 s bins. Blue (triangle) symbols were computed from the two September epoch dwells (Figure 2) showing mHz oscillations, while red (diamond) symbols were computed from intervals immediately following the X-ray burst. A typical error bar is also shown.

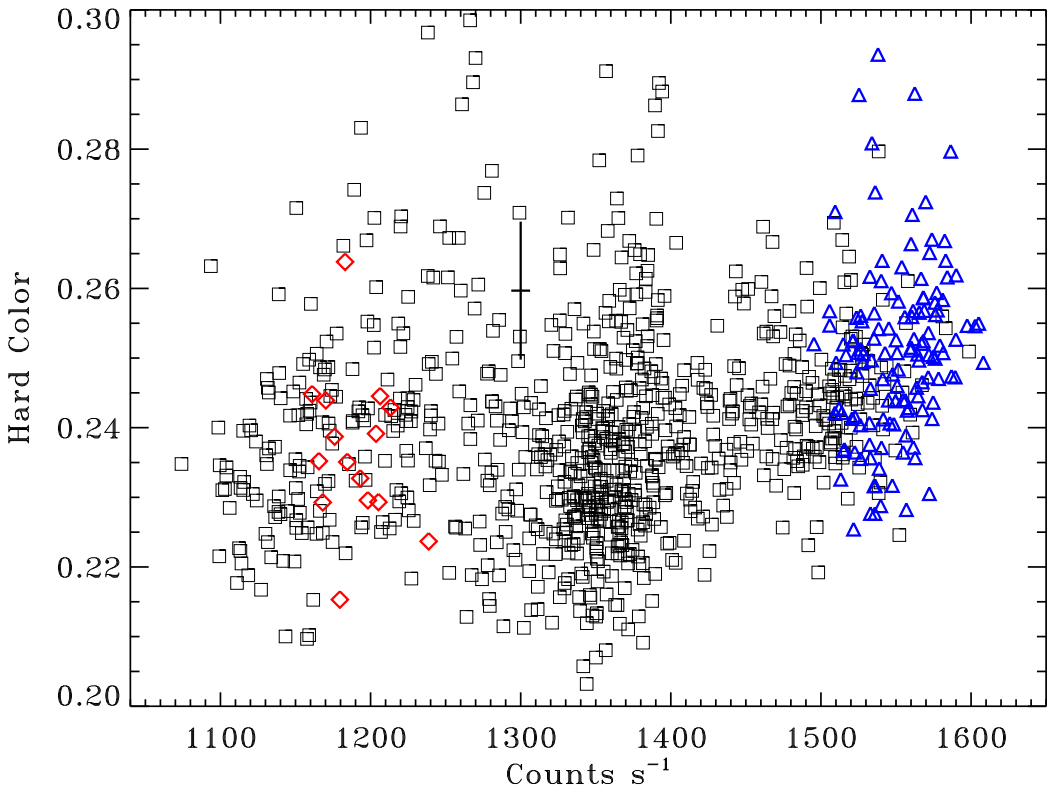


Figure 6. Hardness - intensity diagram of GS 1826 from 34 ks of *NICER* data obtained in the 2017 June, July and September epochs. The hard color is computed as the ratio of count rates in the $5.2 - 6.8$ and $3.5 - 5.2$ keV bands. The intensity is computed using the band $0.5 - 6.8$ keV. Values were computed using 32 s bins. The colored symbols have the same meanings as in Figure 5. A typical error bar is also shown.

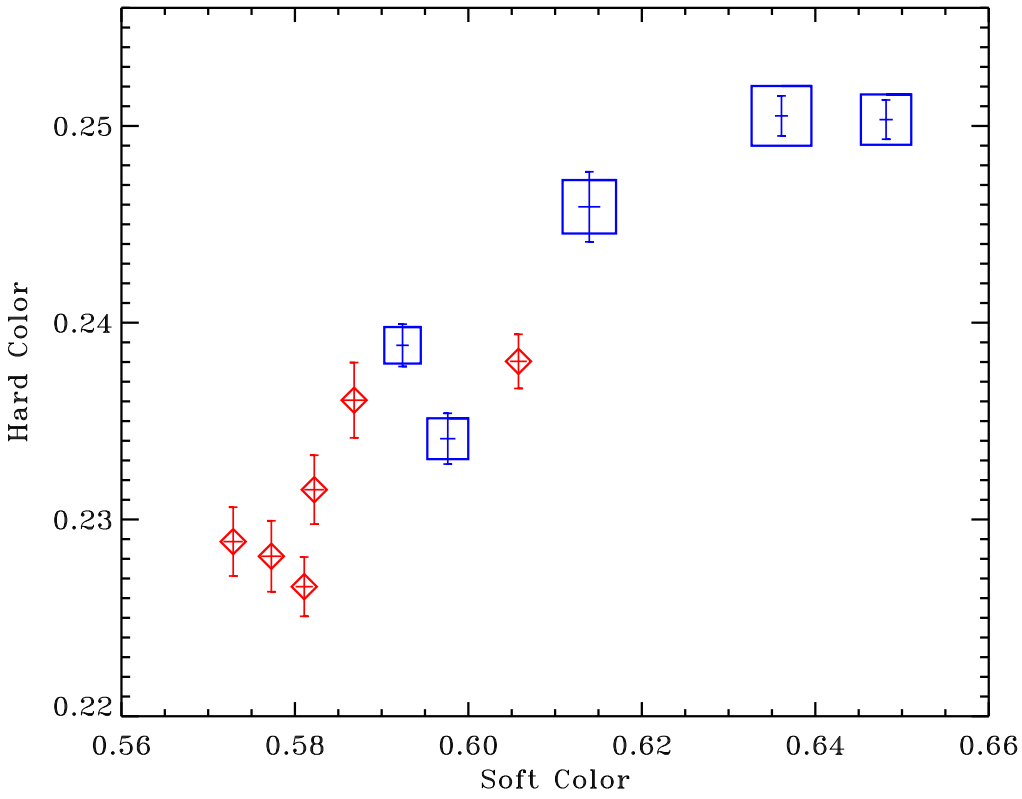


Figure 7. Color - color diagram of GS 1826 from *NICER* dwells in which mHz oscillations were detected (blue square symbols), as well as several dwells for which no mHz oscillations were found (red diamond symbols). For the red diamond symbols, the upper limits to the fractional amplitude (rms) are in the range from 0.4 - 0.5%. For the dwells with mHz detections, the symbol size is proportional to the fractional amplitude (rms).

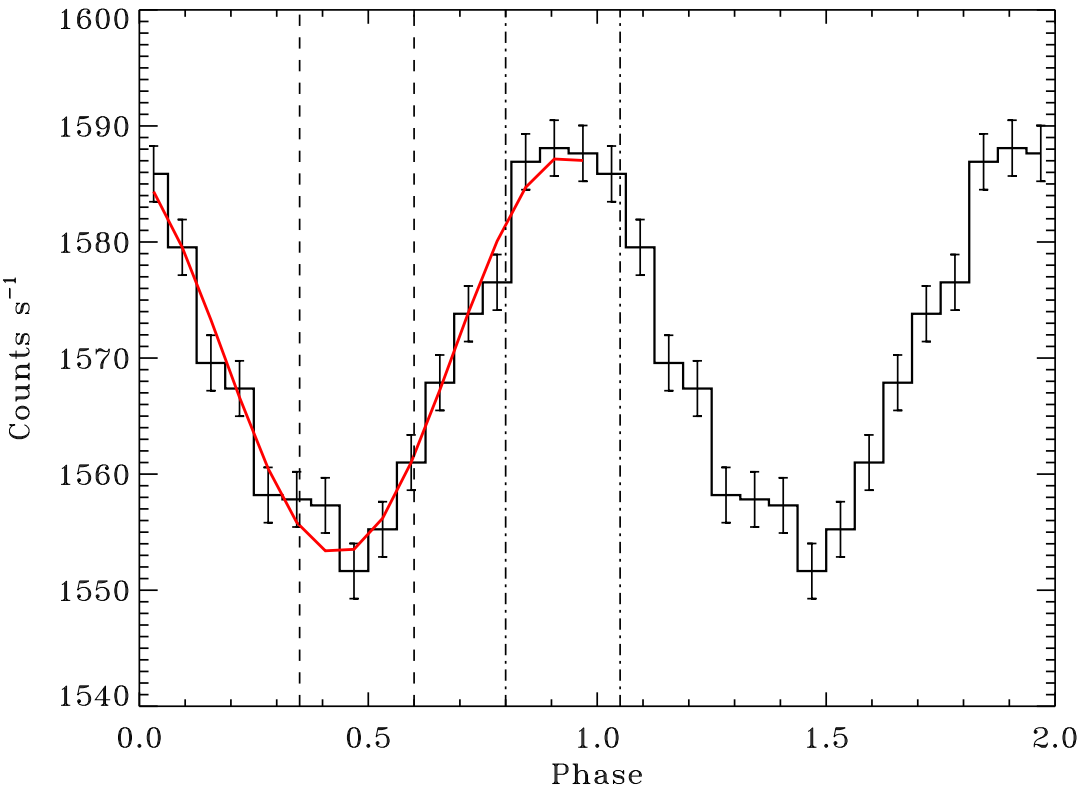


Figure 8. Average, phase-folded mHz oscillation profile from the two *NICER* dwells shown in Figure 2. The profile includes all events in the $0.4 - 7.5$ keV band. The best fitting model, $A + B\sin(\phi - \phi_0)$, is also shown (red curve). Phase ranges used to extract spectra are indicated by the vertical lines. See §3 for additional discussion.

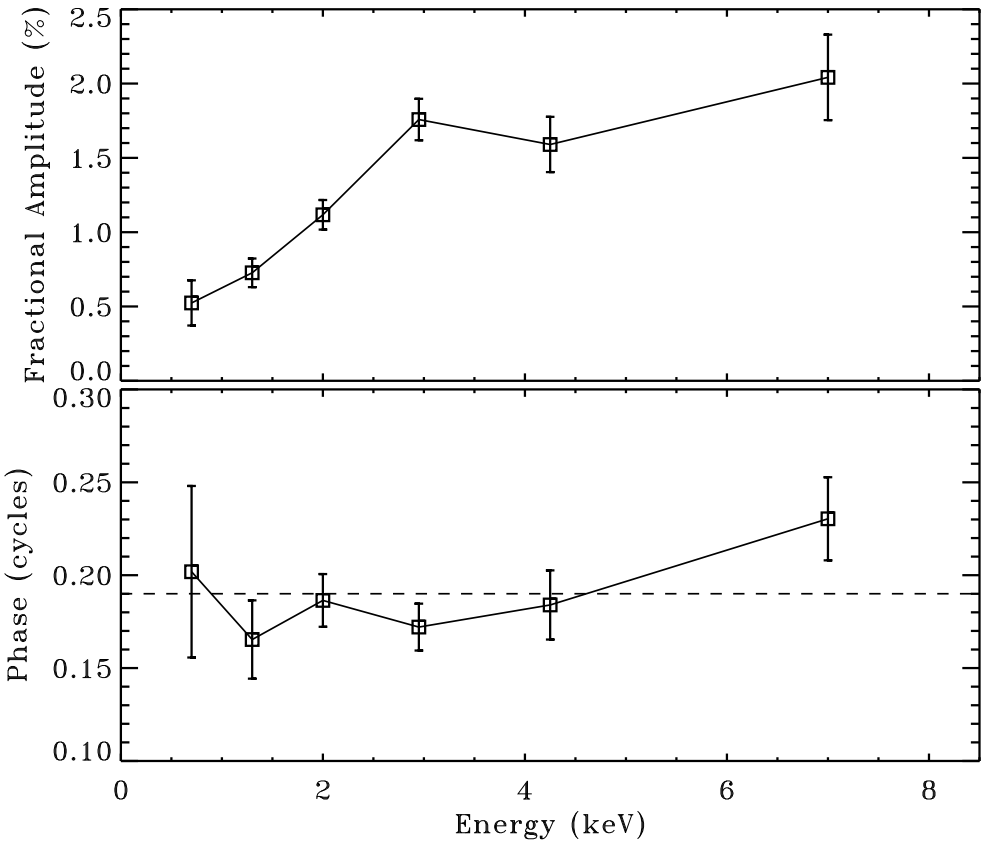


Figure 9. The fractional pulsed amplitude (top) and reference phase, ϕ_0 (bottom), obtained from fits to the phase-folded mHz oscillation profile are shown as a function of energy. The dashed line in the bottom panel marks the mean reference phase value. This constant value provides an acceptable fit to the distribution of values, with a $\chi^2 = 6.9$ for 5 degrees of freedom.

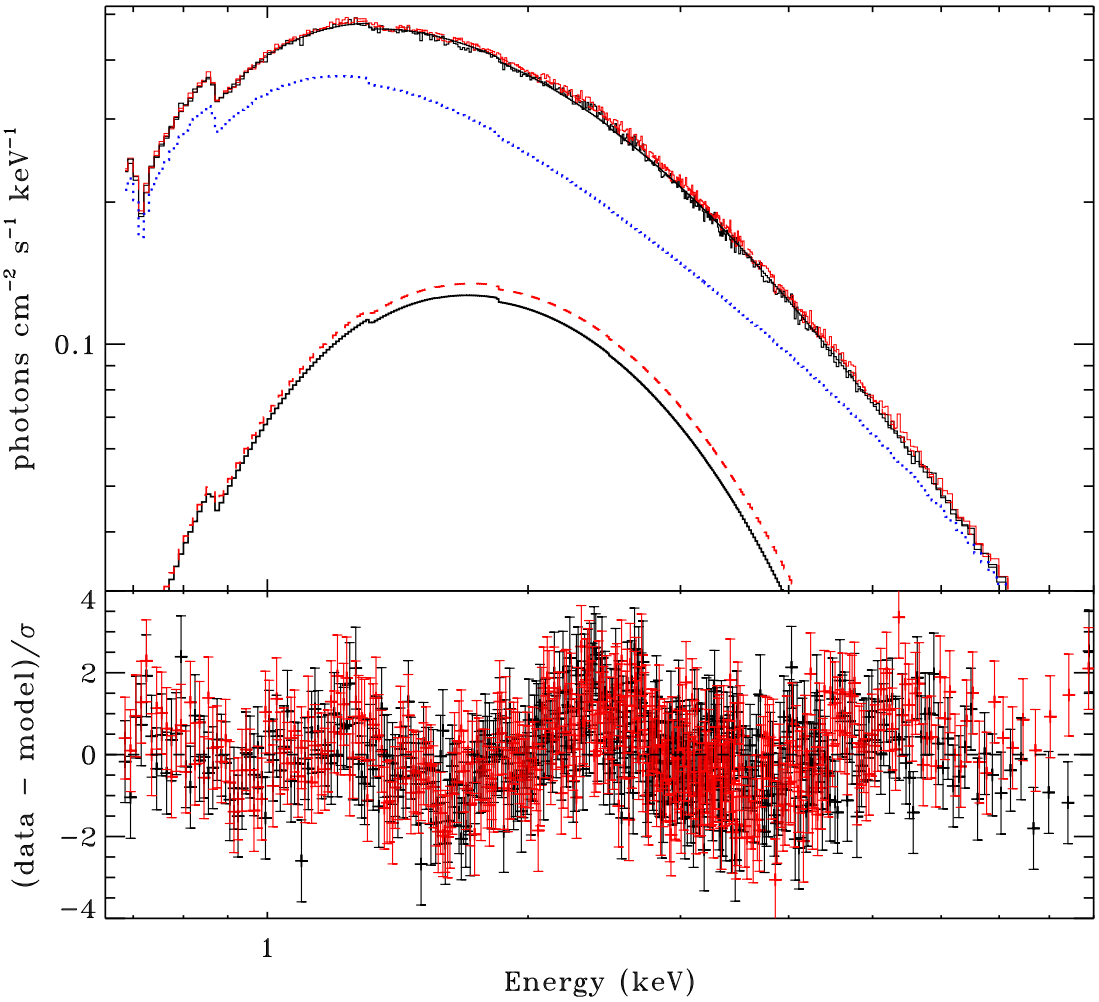


Figure 10. Phase-resolved *NICER* spectra extracted from the minimum and maximum mHz oscillation phases indicated in Figure 6. The unfolded photon spectra are shown along with the total and individual model components (top). The dotted curve between the upper and lower curves is the *comptt* model component, while the two lower curves are the black body *bbodyrad* components. The red and black curves refer to the maximum and minimum phase intervals, respectively. The fit residuals, in units of (data − model)/ σ are also shown (bottom). See discussion in §3 for further details.